

Article

Model Predictive Control for Stabilization of DC Microgrids in Island Mode Operation

Duberney Murillo-Yarce ¹, Sebastián Riffo ², Carlos Restrepo ^{3,*}, Catalina González-Castaño ⁴
and Alejandro Garcés ⁵¹ Engineering Systems Doctoral Program, Faculty of Engineering, Universidad de Talca, Curicó 3340000, Chile² Master in Energy Conversion, Faculty of Engineering, Universidad de Talca, Curicó 3340000, Chile³ Faculty of Engineering, Universidad de Talca, Curicó 3340000, Chile⁴ Department of Engineering Sciences, Universidad Andres Bello, Santiago 7500971, Chile⁵ Department of Electric Power Engineering, Universidad Tecnológica de Pereira, Pereira 660003, Colombia

* Correspondence: crestrepo@utalca.cl

Abstract: DC microgrid (DCMG) is a promising technology for integrating distributed resources, such as solar generation and energy storage devices, that are intrinsically DC. Recently, model predictive control (MPC) is one of the control techniques that has been widely used in microgrid applications due to its advantages, such as transient response and flexibility to nonlinearity inclusion. MPC applications can be centralized, distributed, or decentralized based on the communication architecture. A major disadvantage of the centralized model predictive control (CMPC) is the high computational effort. This paper proposes a CMPC for DCMG stabilization that uses the admittance matrix of a reduced DCMG in the prediction equation and the one-step prediction horizon to decrease the computational effort. The proposed CMPC also replaces the hierarchical architecture primary and secondary controls, achieving voltage or power regulation. A hardware-in-the-loop (HIL) tool, known as RT-Box 2, has been used to emulate an 8-node DC microgrid with versatile buck–boost converters at the supply and power consumption nodes. The proposed predictive control exhibited better performance in comparison with the averaged voltage control in the HIL experiments.

Keywords: centralized communication; DC microgrids; hierarchical control architecture; model predictive control

MSC: 93C95

Citation: Murillo-Yarce, D.; Riffo, S.; Restrepo, C.; González-Castaño, C.; Garcés, A. Model Predictive Control for Stabilization of DC Microgrids in Island Mode Operation. *Mathematics* **2022**, *10*, 3384. <https://doi.org/10.3390/math10183384>

Academic Editor: Nicu Bizon

Received: 9 August 2022

Accepted: 3 September 2022

Published: 18 September 2022

Publisher's Note: MDPI stays neutral with regard to jurisdictional claims in published maps and institutional affiliations.



Copyright: © 2022 by the authors. Licensee MDPI, Basel, Switzerland. This article is an open access article distributed under the terms and conditions of the Creative Commons Attribution (CC BY) license (<https://creativecommons.org/licenses/by/4.0/>).

1. Introduction

A DC microgrid (DCMG) is a promising solution for integrating renewable resources at a low scale [1] and powering electric vehicles, spacecraft, ships, submarines, and telecommunication systems [2–4]. Most distributed energy resources (DER) and energy storage devices are inherently DC, therein the importance of DCMGs in modern systems [5,6]. Another important factor is the increasing use of DC-loads in residential and commercial areas [7]. These loads include lighting systems, computers, servers, data centers, battery chargers, and variable speed drives for heating, ventilation, and air conditioning. Electric vehicles and their charging stations are also DC-loads that may be integrated into a DCMG [8].

A DCMG can operate standalone, or exchange power with the AC distribution system [9]. Regardless of the operation mode, it must operate with high efficiency, stability, and safety standards. Therefore, a specialized control must be designed to achieve these standards. Several control objectives are achievable: voltage regulation, power control, load sharing, loss reduction, energy management, and cost minimization [10]. A hierarchical scheme of three levels is typically adopted to achieve one or several of these objectives [11].

The primary control stabilizes the system at a given operating point, while the secondary control brings the system to the nominal voltage, and the tertiary control achieves economic dispatch. The primary control is decentralized using a droop in power electronic converter [12]. The secondary controller can be centralized, distributed, or decentralized according to its communication links. Generally, centralized and distributed controls require some communication infrastructure [13]. Tertiary control is usually an optimization algorithm that minimizes costs or power loss [14].

Nowadays, model predictive control (MPC) is a popular control strategy, especially in power electronics [15]. MPC uses a mathematical model to predict the system's future behavior in a predefined horizon and select the optima actuation by minimizing a cost function at each sampling step [16]. MPC has outstanding advantages such as fast transient response, flexibility, easy implementation of multiple objectives, and control restrictions for linear and non-linear systems [17,18]. A significant advantage of MPC is that the predicted system outputs may reduce the measurements simplifying the hardware in the implementation stage. Meanwhile, the main disadvantage is the computational complexity when the prediction horizon is high [19].

According to the mathematical model and communication infrastructure, MPC can be centralized, distributed, or decentralized. Distributed and decentralized approaches are helpful to reduce the computational effort [19]. Decentralized controls regulate the voltage at the point of common coupling (PCC) in a scalable and reliable way without communications with other DER [20]. The inclusion of the power converter model in the MPC formulation allows for replacing inner loops and droop control. A decentralized MPC is a suitable solution for the constant power load instability problem [21]. In contrast to decentralized approaches, distributed methods require some communication links. Distributed-MPC requires local measurements and predicted information from its neighbors [22]. MPC execution results in a suboptimal solution in decentralized and distributed strategies since only partial information is available. Instead, an optimal solution can be obtained when all the information is available, as it happens in centralized MPC (CMPC) [23].

There are few publications about CMPC in DCMG. Some works present CMPC controllers that act at the top level of the hierarchical control structure, not requiring a DCMG electrical circuit. For example, the optimal operation of some interconnected microgrids is studied in [23,24], while a CMPC that determines optimal load profiles for electric vehicles is presented in [25]. In the literature, MPC is usually limited to the control of only one DER [26]. In these applications, the control takes into account the model of the power converters that regulate the power exchange between microgrid components. Higher DERs, loads, and the number of storage elements increase the mathematical model complexity. The computational effort reduction is a huge challenge in CMPC.

In the proposed controller in this paper, the high computational effort of predictive controllers is approached in two ways. The first one consists of the mathematical model simplification that is used in the prediction. In the model, a microgrid admittance matrix is used, which is reduced only to those nodes where variable power is injected or absorbed. The other way to reduce computation time is to use a one-step prediction horizon. Regarding the control strategy, this work proposes a CMPC to replace the primary and secondary control of the hierarchical control architecture by a single control strategy. This feature is a novelty since the typical case is to use independent controllers: a droop control on the primary level and a typical control of the secondary level [27]. Additionally, the dynamic model of the DCMG allows to control both voltage and power, prioritizing the variable to control by adjusting a weighting factor.

An additional feature of this work is the validation of the controller on a hardware-in-the-loop (HIL) platform. Usually, the results of the controller's performance at primary and secondary levels in DCMGs are presented only at simulation level. HIL experimentation has been positioned as a significant step in the controllers design for complex systems prior to their implementation in test systems [28]. A HIL tool is used to emulate the

proposed DCMG. Several versatile buck–boost converters are used as an interface to transfer power at the supply and power consumption nodes, which increases the power access and control capability in this DCMG. The versatile buck–boost converter has been presented for different applications, such as fuel cell hybrid power [29,30], automotive traction applications [31], and is proposed as a power electronic building block in [32].

The motivation for this research is the potential that DC microgrids have in integrating renewable energies and the increase in loads that demand energy directly in DC. The scientific community's interest in the study of DC microgrids and the application number is also increasing. This work proposes a new control strategy for DCMG. The main contributions of this paper are as follows:

- A mathematical model simplification for the microgrid is developed in which the admittance matrix is reduced, decreasing the computational effort.
- A single control strategy is developed based on CMPC, which is specialized in replacing the primary and secondary control of the hierarchical control architecture, allowing control of both voltage and power.
- Finally, the use of the same power electronics converter for the interface between the supply and power consumption node is proposed; this technology is the versatile buck–boost converter (VBBC). The VBBC is characterized by high efficiency; variables are easily controllable and can support uni- or bi-directional power flow without hardware modifications. These features make the VBBC suitable for the application.

This paper is organized as follows: Section 2 presents the DCMG model and the controller design. The test model description is presented in Section 3. After, experimental results are shown in Section 4, followed by conclusions in Section 5.

2. DC Microgrid and Control Law

2.1. DC Microgrid Modeling

Figure 1 shows a general representation of a DCMG that integrates renewable and conventional generation, as well as energy storage systems (ESS) and different types of loads. The DCMG can connect to the AC grid to supply or absorb power. Power converters connect sources, loads, and energy storage units to the DC bus. Each node can be represented by a power source (p_n) in parallel with a capacitor (c_n) and admittance (g_n), as shown in Figure 2a. The power source represents the supply or power consumption. The capacitor represents the capacitive effect of the connecting cables and the equivalent capacitance of the converter that connects the node to the DC bus, and the admittance represents losses.

For analysis purposes, it is convenient to obtain a reduced model of the DCMG limited to those nodes of variable power where there are power electronics converters capable of stabilizing the microgrid after any change in the operating conditions. The admittance matrix reduction is carried out by applying the Kron reduction, a standard tool in the electrical systems community. For analysis purposes, it is convenient to obtain a reduced model of the DCMG limited to those nodes of variable power where there are power electronics converters capable of stabilizing the microgrid after any change in the operating conditions. From the point of view of circuit theory, a lower-dimensional electrically-equivalent circuit is obtained [33]. The Kron procedure eliminates the nodes of constant power, as described in [34]. The result of the reduction is an equivalent admittance matrix (G) that implicitly has the characteristics of the original topology. This matrix considers all the resistive effects of the DCMG, including node and line admittances. Then, each model node in the equivalent DCMG can be reduced to a source and a capacitor, as shown in Figure 2b. The dynamic model of node n in Figure 2b is obtained by applying Kirchhoff's Current law, as given in (1), where v_n is the voltage of node n voltage and i_n is the current injected to the microgrid from the node n . As i_n depends on the line admittances and the node voltages, (1) can be rewritten as (2). In this equation, M is the total number of nodes of the equivalent DCMG, g_{nm} is the admittance joining node n to node m , and v_m is the voltage of node m .

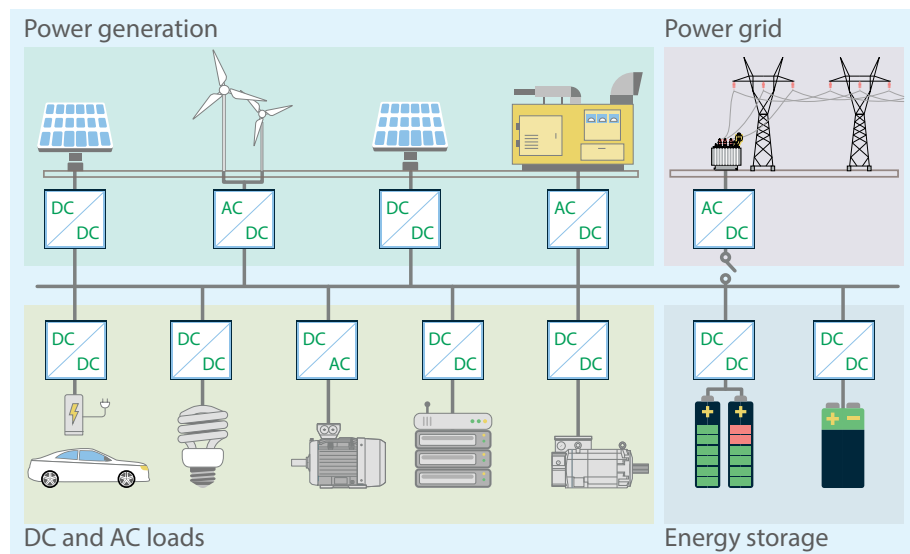


Figure 1. General topology of a DCMG.

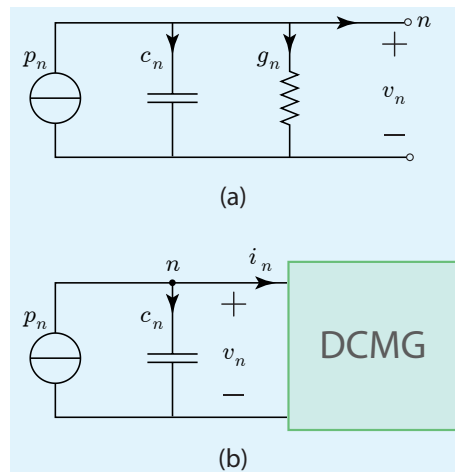


Figure 2. Model of a node in the DCMG: (a) general model, (b) equivalent model.

$$\frac{p_n}{v_n} = c_n \frac{dv_n}{dt} + i_n. \tag{1}$$

$$\frac{dv_n}{dt} = \frac{1}{c_n} \left(\frac{p_n}{v_n} - \sum_{m=1}^M g_{nm} v_m \right). \tag{2}$$

Equation (2) can be represented in matrix form as follows,

$$\frac{dV}{dt} = C^{-1} \left((\text{diag}(V^{-1}))P - GV \right), \tag{3}$$

where V is the node voltages vector, C is the capacitance matrix, P is a vector with the value of the controlled power by each DC–DC converter, and G is the nodal admittance matrix. The matrix $\text{diag}(V^{-1})$ denotes the diagonal matrix of $\frac{1}{V}$.

2.2. Model Predictive Control

MPC uses physical system information to predict future evolution and evaluates a suitable cost function. The control signal for the next interval is defined by that sequence which minimizes future error in the output. The prediction is realized using the mathematical model of the dynamic system. The control output is updated at each sampling instant

with corrections based on the new information. The main stages of the MPC methodology are shown in Figure 3.

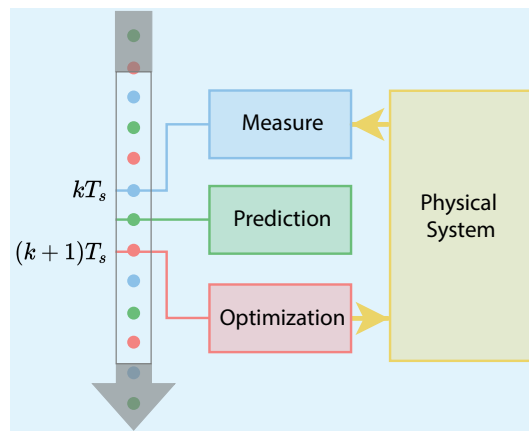


Figure 3. Main stages of MPC algorithm.

Prediction of the system future outputs is made using a prediction horizon. For a prediction horizon N , the future outputs y_k for $k = 1 \dots N$ are predicted from known values and future control signals u_k for $k = 1 \dots N - 1$. The control signals are calculated through an optimization process that minimizes the future output error.

2.3. Controller Design

A conventional MPC requires a high computational cost that depends on the prediction horizon. This research aims to design a controller with low computational effort and minimum response time. The deadbeat control is a particular case of the MPC, which is characterized by eliminating the error in the next sampling time. The deadbeat control satisfies the design criteria optimally. The controller model presented in (4) is obtained through the discretization of the dynamic model given in (3). k is the current time instant.

$$\frac{dV_k}{dt} = C^{-1}(\text{diag}(V_k^{-1}))P_k - C^{-1}GV_k. \tag{4}$$

The discrete derivative for the sampling time T_s can be expressed as in (5). Substituting (5) in (4) results in (6), which is the prediction equation for V .

$$\frac{dV_k}{dt} = \frac{V_{k+1} - V_k}{T_s}. \tag{5}$$

$$V_{k+1} = (I - T_s C^{-1}G)V_k + T_s C^{-1}(\text{diag}(V_k^{-1}))P_k. \tag{6}$$

Considering definitions (7) and (8), (6) can be rewritten as (9). This equation is equivalent to the state variable representation. It can be noted that it is a non-linear model.

$$A = I - T_s C^{-1}G. \tag{7}$$

$$R = T_s C^{-1}(\text{diag}(V_k^{-1})). \tag{8}$$

$$V_{k+1} = AV_k + RP_k. \tag{9}$$

The next step is to define the cost function J . The proposed cost function is shown in (10). This function is a quadratic expression that depends on V and P . \bar{V} and \bar{P} are the reference values of V and P . Note also that there are two weighting diagonal matrices Q

and S in the cost function, whose purpose is to give priority to V or P , respectively. Q and S are positive definite matrices. Substituting (9) in (10), Equation (11) is obtained.

$$J = \frac{1}{2}(V_{k+1} - \bar{V})Q(V_{k+1} - \bar{V}) + \frac{1}{2}(P_k - \bar{P})S(P_k - \bar{P}). \tag{10}$$

$$J = \frac{1}{2}(AV_k + RP_k - \bar{V})Q(AV_k + RP_k - \bar{V}) + \frac{1}{2}(P_k - \bar{P})S(P_k - \bar{P}). \tag{11}$$

Equation (12) is obtained by differentiating, with respect to P_k , the cost function in (11).

$$RQ(AV_k + RP_k - \bar{V}) + S(P_k - \bar{P}) = 0. \tag{12}$$

Finally, P_k that minimizes the cost function in one-step is given by:

$$P_k = -(RQR + S)^{-1}(RQAV_k - RQ\bar{V} - S\bar{P}), \tag{13}$$

where $Q = (1 - \alpha)(\text{diag}(1/\bar{V}^2))$ and $S = \alpha(\text{diag}(1/\bar{P}^2))$, being α a weighting factor that must be adjusted to minimize voltage or power tracking. Note that the condition $0 < \alpha < 1$ is satisfied.

3. Test Model

This section first describes the test model used to validate the proposed controller. The test model consists of an 8-node DCMG that integrates elements such as loads, sources, and ESS, which are connected to a DC bus through DC–DC converters. Second, the control scheme is described by focusing on the study case.

3.1. Proposed DCMG

The proposed DCMG for experimental validation of the control algorithm is shown in Figure 4. The test system corresponds with an 8-node microgrid that can operate connected to a grid or in islanded mode [34]. The microgrid study in this article corresponds to an off-grid system based on 2000 W photovoltaic installed capacity and an energy storage unit with one day of autonomy. The energy processing can provide electricity to two loads of constant power, and one of variable power, whose power rating values are shown in Table 1. Electrical wires are sized according to the maximum power, and the DC-bus voltage reference. Two electrical wire types are used: (i) AWG 12, 25 A, 5.2 Ω/km, and (ii) AWG 8, 50 A, 2.1 Ω/km. The parameters of the connection lines between nodes are listed in Table 2, where the resistance value per length unit depends on the wire gauge. The microgrid elements are located as shown in Figure 4:

- Source: photovoltaic solar system connected at node 3.
- Loads: one controlled DC-load connected in node 5 and constant power loads (CPLs) in nodes 2 and 8.
- Energy storage system: 48 V battery connected at node 7.

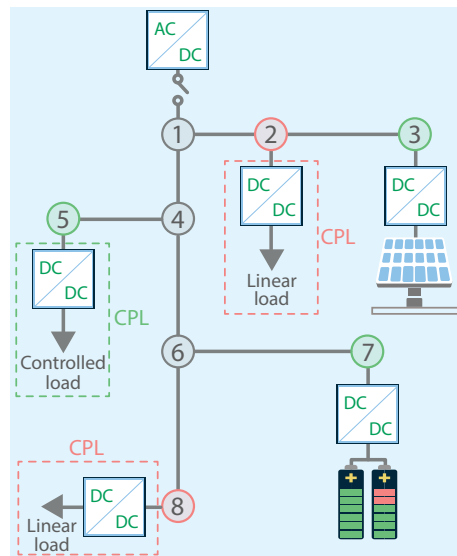


Figure 4. Proposed DCMG for experimental validation.

Table 1. The load’s rated values.

Node	Description	Power
2	Constant power load	300 W
5	Controlled load	Pmax. 1000 W
8	Constant power load	500 W

Table 2. Parameters of the connection lines between nodes.

Node From	Node to	Resistance (Ω/km)	Length (m)
1	2	2.1	10
2	3	2.1	25
1	4	2.1	5
4	5	5.21	22
4	6	2.1	8
6	7	2.1	20
6	8	5.21	16

Intermediate nodes are eliminated to simplify the mathematical model of the DCMG, and constant power terminal nodes are also reduced using the Kron procedure. Thus, the grid is reduced to a 3-node system that includes power electronic converters (nodes 3, 5, and 7), as shown in Figure 5. The equivalent matrix G of the reduced DCMG is:

$$G = \begin{pmatrix} 8.1924 & -2.7410 & -5.3295 \\ -2.7410 & 6.7106 & -3.9158 \\ -5.3295 & -3.9158 & 9.4106 \end{pmatrix}. \tag{14}$$

3.2. DC–DC Power Converters

The connection of the microgrid elements to the DC bus is carried out using DC–DC converters that execute the control laws to guarantee stability. Classical buck, boost, and buck–boost converters have been widely used in DCMG. Buck and boost topologies can only step down or step up voltage, respectively. In contradistinction, buck–boost topology can perform both buck or boost functions, suitable for DC voltage regulation applications in intermediate values.

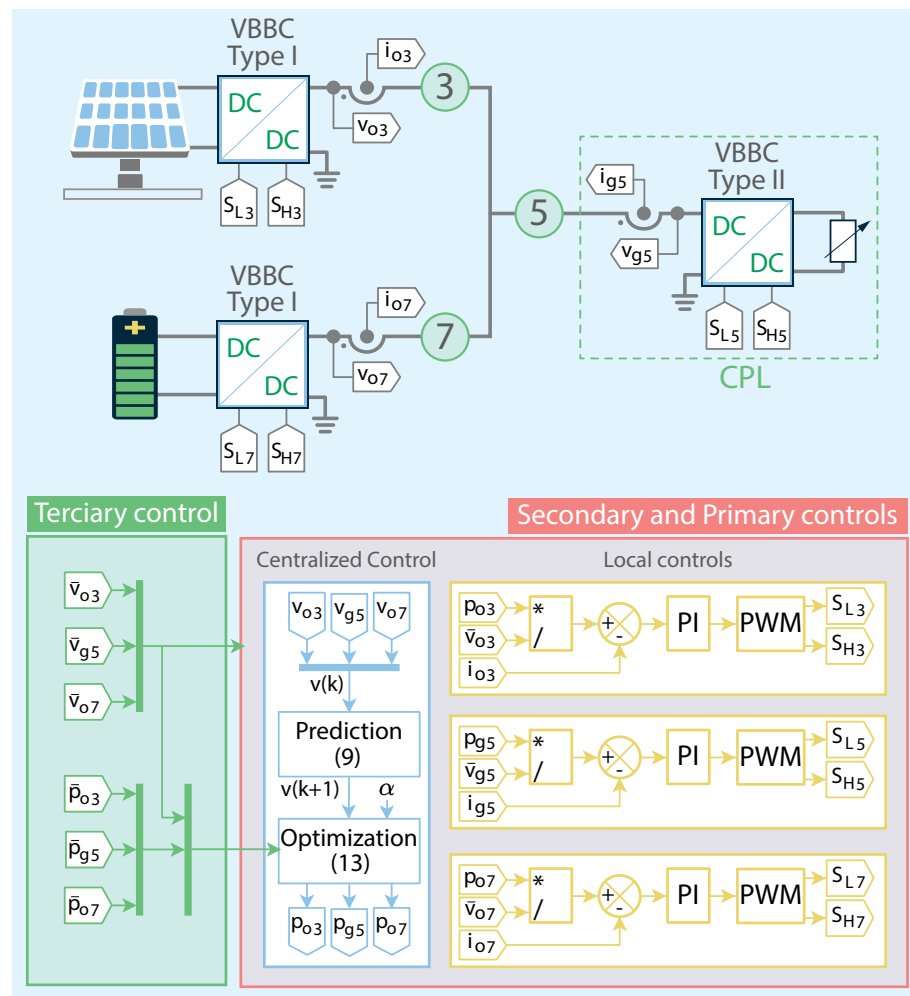


Figure 5. Reduced test model and general control scheme.

Unidirectional converters are classic components in DCMG often used for connecting DER and loads to DC bus. On the other hand, bidirectional converters have received much attention due to the ESS, which may deliver or store power. ESS provides greater flexibility to the DCMG operation. It is recommended to connect the ESS to the DC bus through bidirectional DC–DC converters to avoid inrush current, fluctuations in the DC-bus voltage, and the loss of ESS lifetime [8]. Another situation where bidirectional converters are required is the connecting of microgrids with different bus voltage levels [35].

For the connection of variable power nodes with the DC bus, the non-inverting buck–boost converter of coupled inductors was used, known in the literature as a versatile buck–boost converter (VBBC) due to its outstanding characteristics. This converter was initially presented in the literature in [36]. The VBBC is also characterized by its large bandwidth and non-pulsating currents at the input and output. This converter is ideal for stabilizing DCMG because it allows controlling both currents and voltages at the input or output [37]. These characteristics become the VBBC in a building block that can connect both sources and loads to the DC bus. The VBBC can operate in both boost and buck mode. One of the main power MOSFETs (Q_1, Q_2) switches to high frequency while the other is opened or closed. In boost, Q_1 switches and Q_2 is closed, while in buck, Q_2 switches and Q_1 is in the open state. The secondary MOSFETs Q_3 and Q_4 operate in complementary states to the MOSFETs Q_1 and Q_2 .

The possible power circuits of the VBBC are shown in Figure 6. In the VBBC topology, there is an inductor that can be located at the output (Figure 6a) or the converter input (Figure 6b), according to the control requirements. In the source nodes, the inductor acts as an output filter to reduce the current ripple injected into the DC bus, while the inductor as

an input filter is useful in the load nodes to reduce the absorbed current ripple from the bus. The VBBC components are: $R_d = 0.5 \Omega$, $C = 200 \mu\text{F}$, $C_d = 100 \mu\text{F}$, $C_i = 20 \mu\text{F}$, $L = 47 \mu\text{H}$, and $L_m = 12 \mu\text{H}$. Information about the design of the VBBC converter can be found in [37].

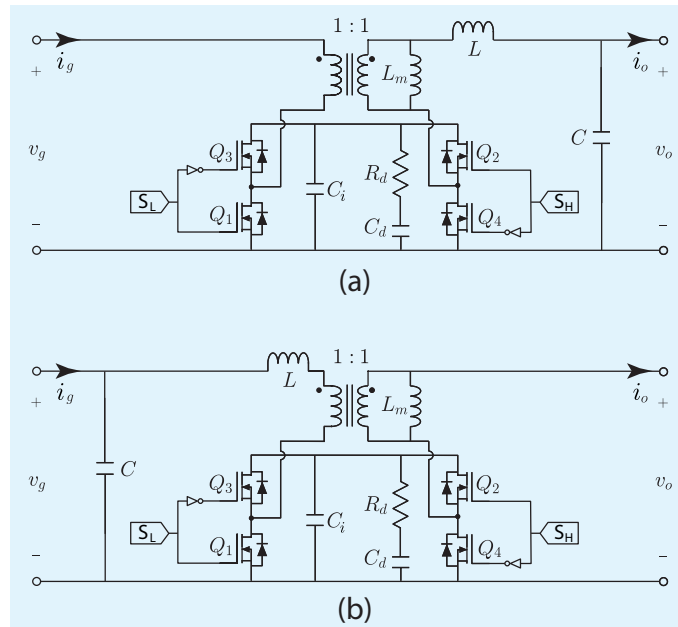


Figure 6. Power circuit VBBC with: (a) output filter, (b) input filter.

It can be noticed in Figure 6 that the subscripts g and o refer to variables at the converter input and output port, respectively. This notation will be used in future figures.

3.3. CMPC Applied at Test Model

To decrease the computational effort in the control law implementation, the 8-node DCMG was reduced to a 3-node DCMG. The reduced DCMG is shown in Figure 5. The nodes that remain in the equivalent DCMG are: (i) node 3 (source), (ii) node 5 (variable load), and (iii) node 7 (energy storage).

If it is considered an initial condition where the battery connected to node 7 has been previously charged, nodes 3 and 7 can be designated as source nodes. Therefore, elements in nodes 3 and 7 are connected to the DC bus through a VBBC converter with an output filter (see Figure 6a) that regulates supplied power. On the other hand, node 7 can be designated as a load node, and the element in node 7 is connected to the DC bus through a VBBC converter with an input filter (Figure 6b) to regulate the absorbed power. Controlled variables at source and load nodes are those at the converter port connected to the DC bus, as shown in Figure 5. This figure also describes the general control scheme regulating voltage and power in nodes 3, 5, and 7. The tertiary control sets the references of the controllers below in the hierarchical control structure. The proposed CMPC develops secondary and primary controls. In addition, a local control based on a proportional–integral (PI) control sets the switching signals of the VBBC. The PI parameters are $k_p = 0.0325$ and $T_i = 0.0009$.

3.4. Local Control of CPLs

CPLs belong to load nodes, then the controlled variables are at the converter input port, as shown in Figure 7. This figure also describes the proposed local control for power regulation. It consists of a droop control in cascade with a classic double-loop control (inner current loop and outer voltage loop).

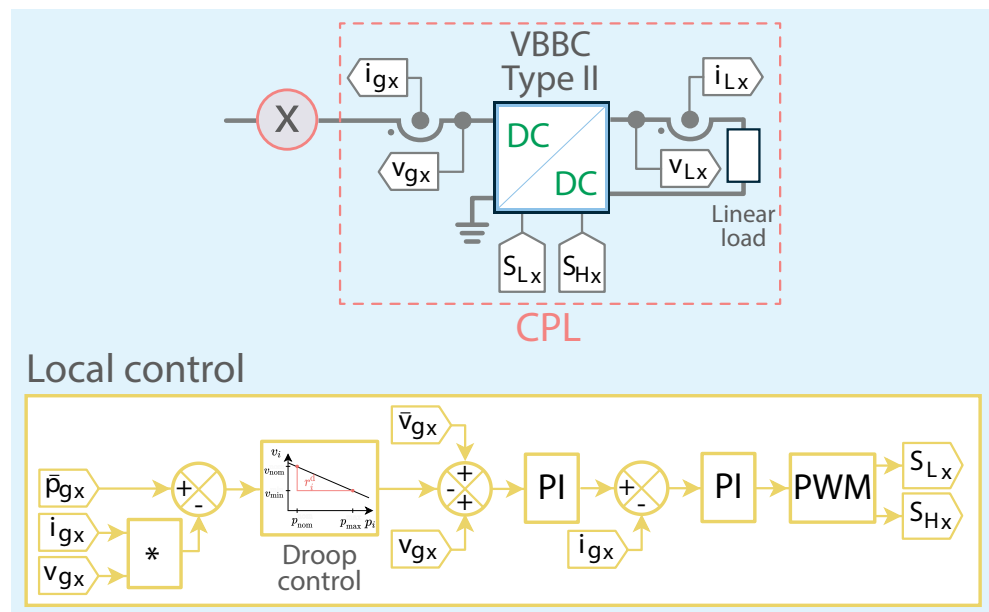


Figure 7. Local control for power regulation in CPLs.

The droop control defines the operation region of the point (p, v) as shown in Figure 7. The droop control is completely defined by the slope (r_d) of the straight line that relates to both variables. r_d is known as droop constant and is given by (15).

The CPL controller parameters are listed in Table 3. Further, x in Figure 7 is the corresponding node, fulfilling that $x \in \{2, 8\}$.

$$r_d = \frac{\Delta v}{\Delta p} = \frac{v_{nom} - v_{min}}{p_{max} - p_{nom}} \tag{15}$$

Table 3. Local controller parameters of CPLs.

Loop	Constant	Value
Droop	r_d	-0.04
Voltage	k_p	0.75
	T_i	0.0004
Current	k_p	0.0325
	T_i	0.0009

4. Results

The proposed controller has been validated using hardware-in-the-loop (HIL). HIL tools have become very popular in the controller design and validation stages. HIL can emulate parts of the test system such as controllers, power converters, or the power systems where the converters are integrated [38]. This reason makes HIL tools especially useful in microgrid applications. The experimental setup based on HIL is shown in Figure 8.

The experimental results show the evolution of the voltages, currents, and powers in the nodes of the reduced DCMG (nodes 3, 5, and 7) from a null initial condition to a steady-state condition. The reference voltage remains fixed at 48 V, and the power references change from an initial to a final one dataset defined as Test1 and Test2, which are listed in Table 4. It is essential to mention that the sign convention used for current and power is a positive sign for sources and a negative sign for loads. Moreover, the sampling period (T_s) is 40 μ s.

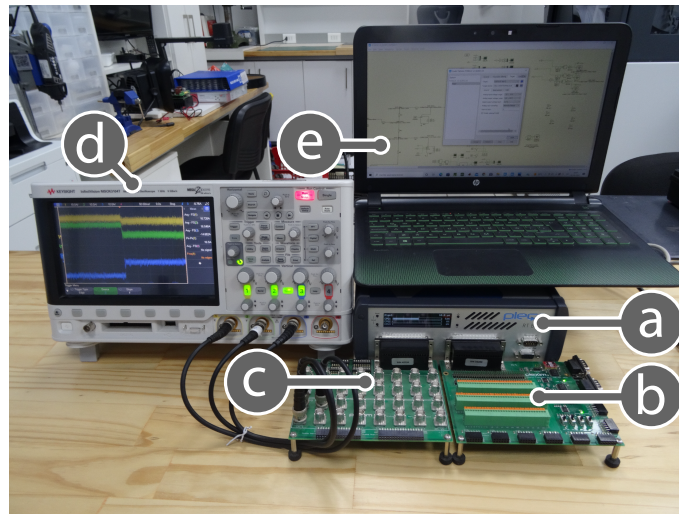


Figure 8. Experimental setup based on HIL: (a) PLECS RT-Box 2, (b) RT-Box digital breakout board, (c) RT-Box analog breakout board, (d) oscilloscope, (e) laptop for programming the RT-Box 2.

Additionally, the proposed MPC controller performance is compared with the average voltage control.

Table 4. Active power references in Watts (W).

Node	Test1	Test2
3	800	700
5	−900	−300
7	1000	500

4.1. Model Predictive Control

The weighting factor α must be conveniently defined to apply the proposed control law (Equation (13)). α allows the controller to prioritize between voltage or power tracking. Figure 9a,b show the root mean square error (RMSE) of voltage and power tracking as a function of the factor α . The power references in Figure 9a,b are, respectively, the sets Test1 and Test2, while the DC-bus voltage reference is 48 V in both cases. Figure 9a,b show that α , which minimizes the power RMSE for Test1 and Test2, are 0.16 and 0.09, while $\alpha = 0$ minimizes the voltage tracking.

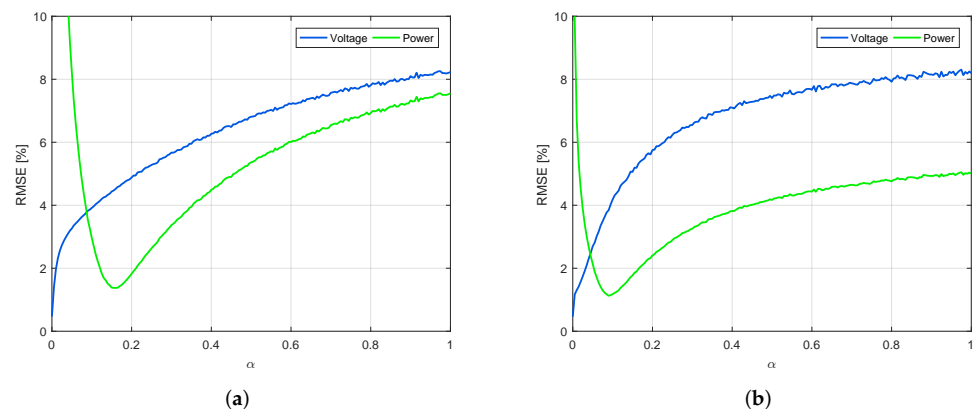


Figure 9. Voltage and power tracking RMSE for 48 V and power references: (a) Test1, (b) Test2.

4.2. Average Voltage Control (AVC)

The average voltage, operating in conjunction with a droop control, is proposed to compare the predictive controller. The average voltage is a distributed secondary technique

of the hierarchical control scheme. Droop control is a classic control at the primary level. It is a proportional controller, so it operates with a steady-state error. The droop control response is modified by the AVC technique to reduce the steady-state error. Each converter measures its voltage and then communicates it with the other converters to modify this gain. Thus, every converter, or most of them, will have the measured voltage of its neighbors. Then, using the global average of these voltages, each converter computes its control signal, modifying the droop gain. Finally, the globally average voltage of the converters will follow the bus voltage reference. The block diagram of the joint operation of both techniques is shown in Figure 10. The controller parameters are: $k_i = 100$ and $r_d = -0.04$.

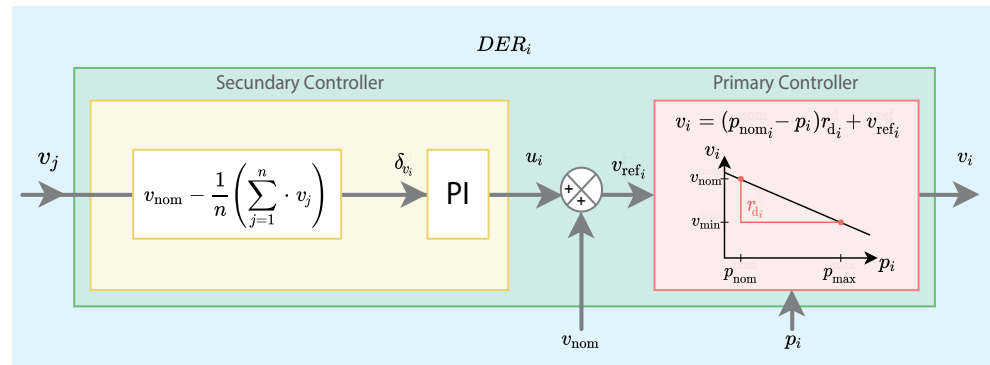


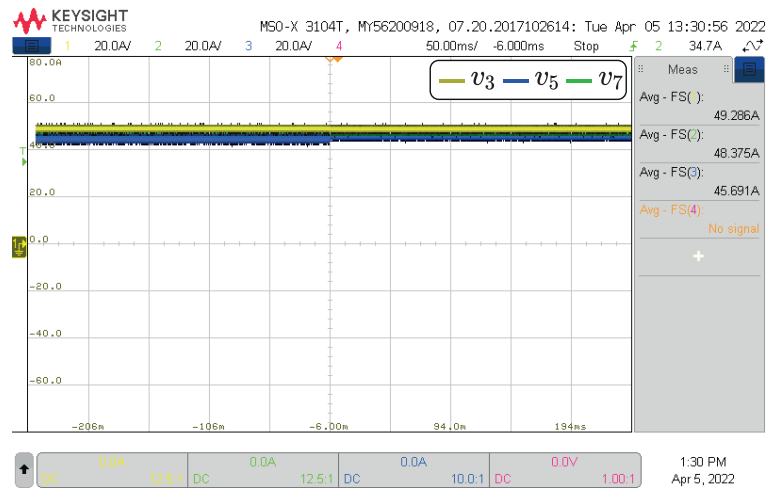
Figure 10. Average voltage control scheme.

4.3. Results and Comparison

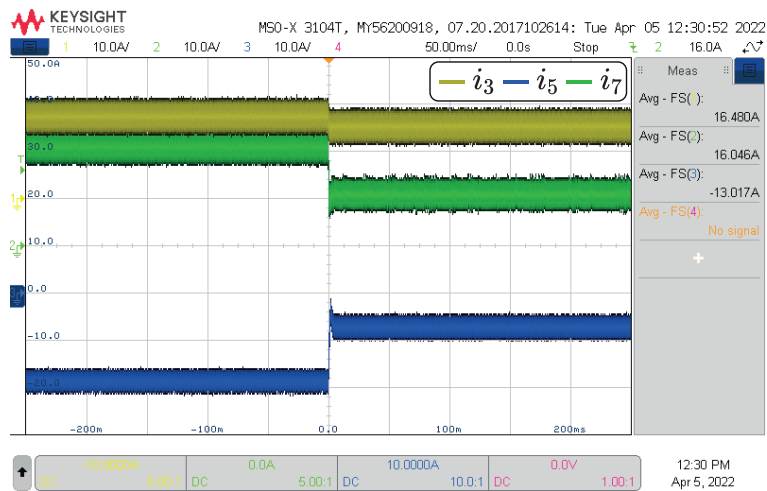
Experimental results are shown in Figures 11–15. The first test evaluates the controller performance to a power reference change. Figures 11 and 12 show results from CMPC and AVC, respectively. In both cases, the nodes’ voltage, current and power responses are shown for a reference change from dataset Test1 to Test2. The average results are shown in Tables 5–7. Waveforms in Figures 11 and 12 depict that both controllers exhibit similar behavior in steady-state. The average powers obtained by the controllers for each reference, which are listed in Table 7, show that the CMPC performs a better power tracking. This observation is based on the errors (RMSE) listed in Table 7, where it can be seen that the maximum errors of the CMPC and the AVC control are 1.5% and 5.6%, respectively. Regarding the transient responses, the CMPC exhibits a shorter settling time, while the AVC shows a higher overshoot in conjunction with a high-frequency oscillatory component. In addition, the waveforms obtained by applying CMPC present a uniform ripple, while the responses of AVC present a non-uniform ripple and high noise content.

The next test shows a comparison between the proposed CMPC and the AVC. This test achieves the power references defined by the dataset of Test1, starting from null initial conditions. The start-up voltage, current and power responses in nodes 3, 5, and 7 are shown in Figure 13 for CMPC, and Figure 14 for AVC. Figure 13c shows how the proposed CMPC rapidly follows the given power references without overshoot, while the AVC presents a damped response and a longer settling time, as shown in Figure 14c. The settling time of the CMPC and AVC are 4 ms and 60 ms, respectively.

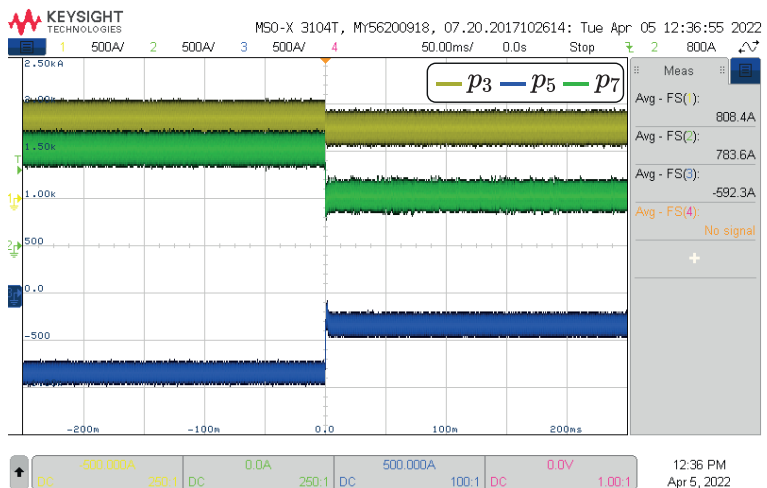
In general, the good dynamic response of the proposed CMPC is validated both at start-up and the reference change. The controller reaches the reference without overshoot and in a minimum time in both cases. On the other hand, the AVC controller presents a damped behavior in transitions. This behavior depends on the internal PI controller-tuning of the AVC. Then, adjusting the PI constants can achieve a balance between settling time and overshoot.



(a)

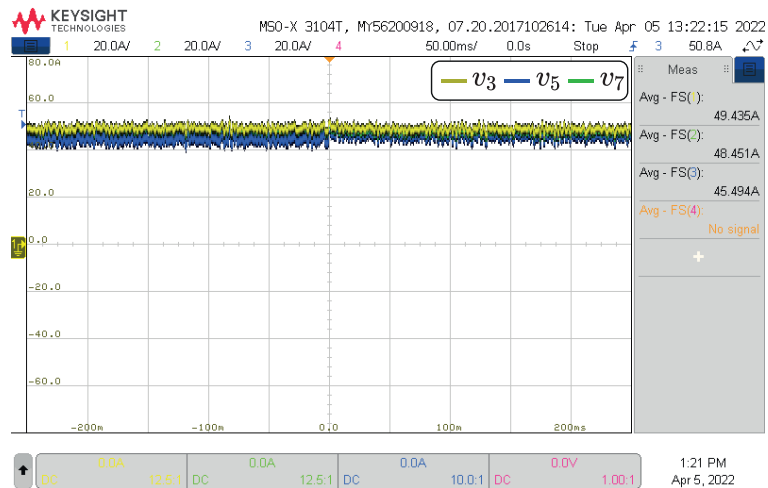


(b)

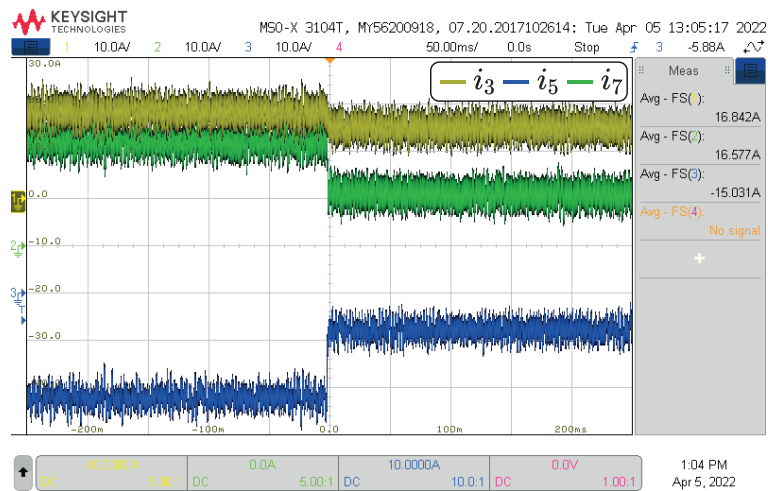


(c)

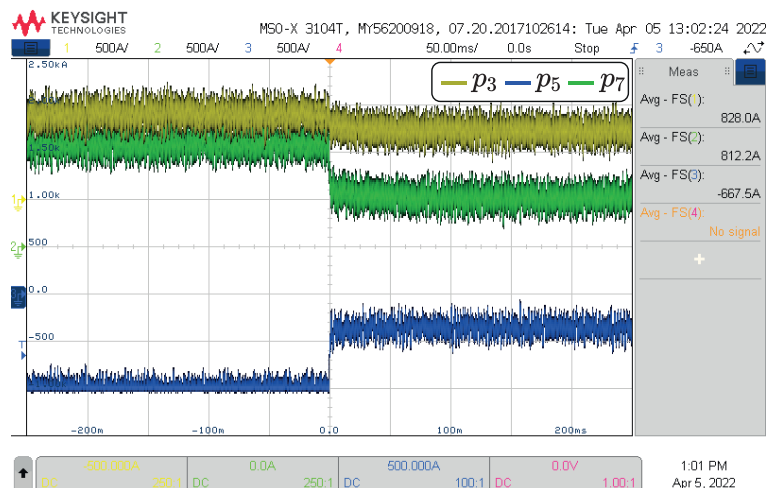
Figure 11. Performance of the model predictive control proposed to a power reference change: (a) voltage (10.0 V/div), (b) current (10.0 A/div), (c) power (10.0 W/div). Time base of 50 ms/div and DC coupling.



(a)

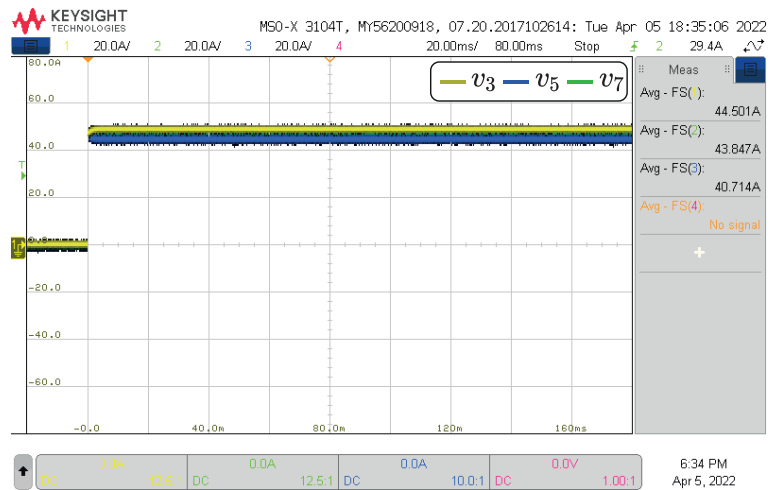


(b)

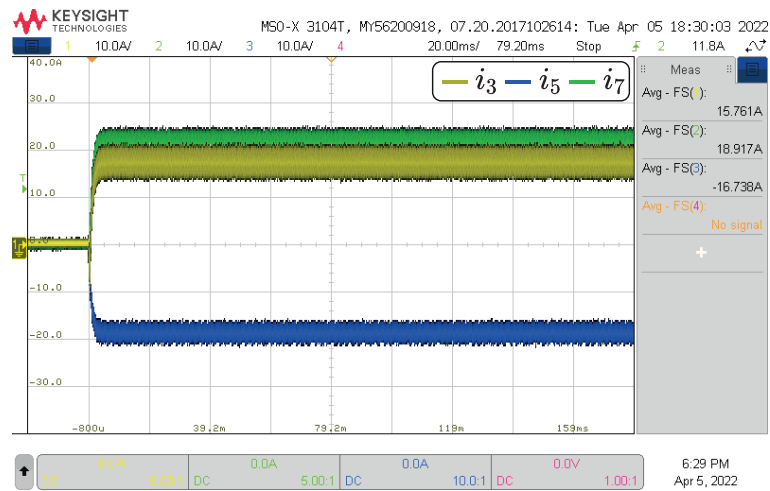


(c)

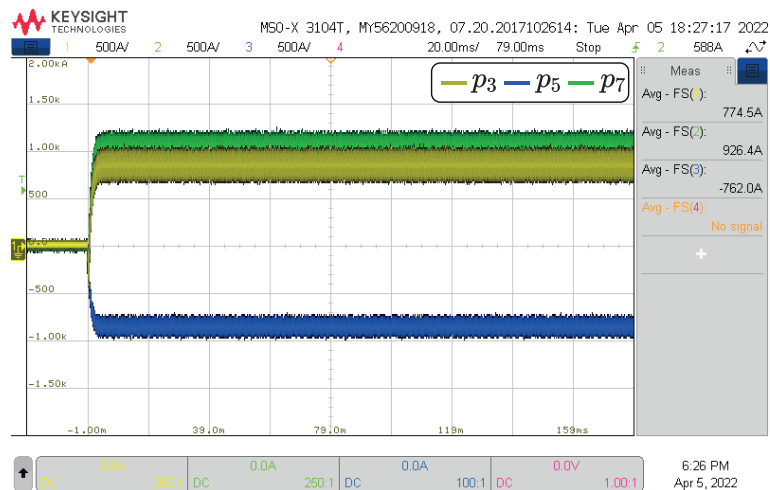
Figure 12. Performance of the average voltage control to a power reference change: (a) voltage (10.0 V/div), (b) current (10.0 A/div), (c) power (10.0 W/div). Time base of 50 ms/div and DC coupling.



(a)

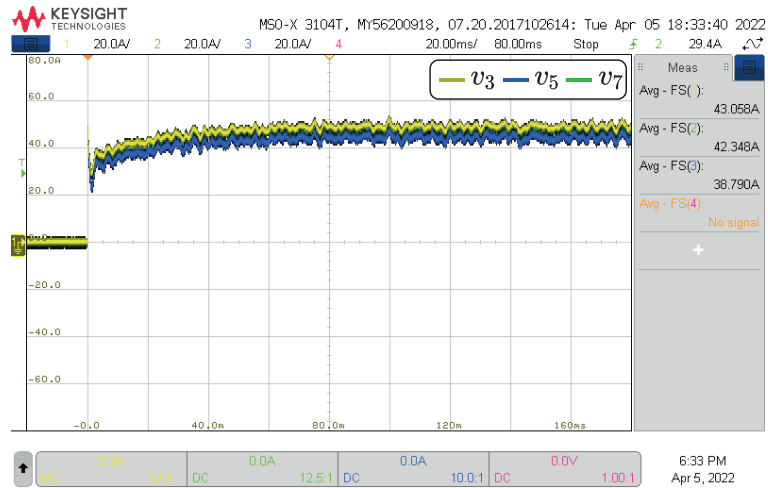


(b)

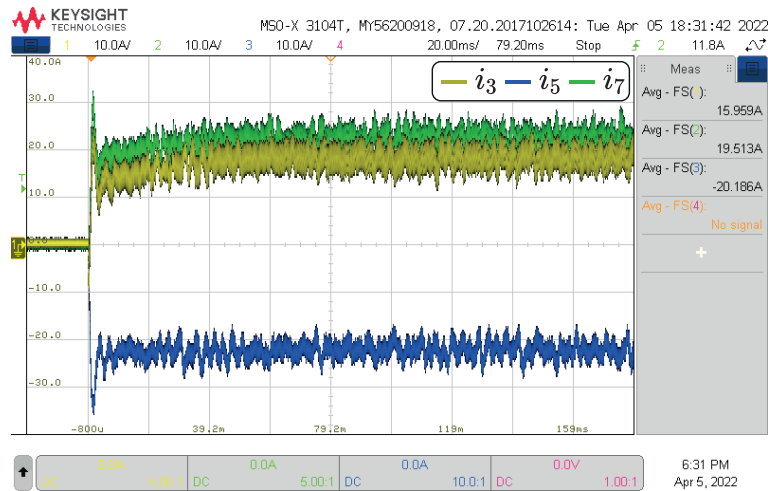


(c)

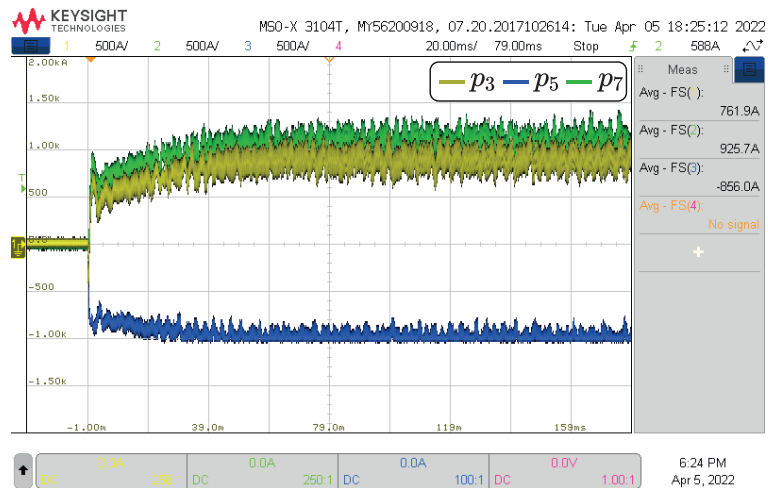
Figure 13. Model predictive control start-up responses: (a) voltage (10.0 V/div), (b) current (10.0 A/div), (c) power (10.0 W/div). Time base of 20 ms/div and DC coupling.



(a)

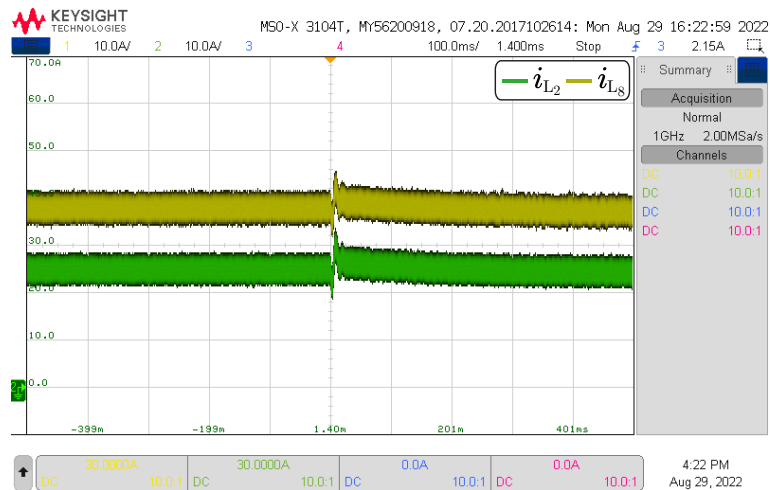


(b)

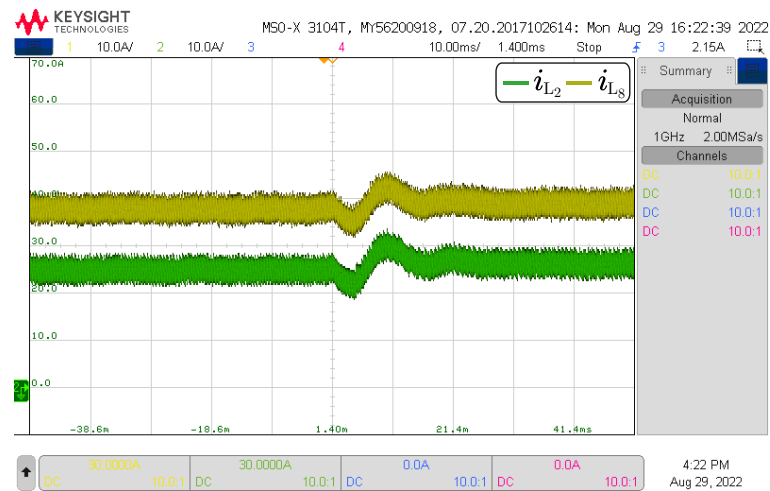


(c)

Figure 14. Average voltage control start-up responses: (a) voltage (10.0 V/div), (b) current (10.0 A/div), (c) power (10.0 W/div). Time base of 20 ms/div and DC coupling.



(a)



(b)

Figure 15. Currents waveform in CPLs at nodes 2 and 8 under power sudden change: (a) timebase 100 ms/div, (b) timebase 10 ms/div. (10.0 A/div).

Table 5. Average voltage results in volts (V) for CMPC and AVC controllers.

Node	CMPC		AVC	
	Test1	Test2	Test1	Test2
3	50.6	50.4	49.3	48.7
5	47.3	48.7	45.6	47.0
7	50.4	49.8	49.1	48.2

Table 6. Average current results in amperes (A) for CMPC and AVC controllers.

Node	CMPC		AVC	
	Test1	Test2	Test1	Test2
3	16.0	13.7	16.9	13.3
5	-18.5	-6.5	-21.6	-6.8
7	19.8	10.1	21.1	9.6

Table 7. Average power results in watts (W) for CMPC and AVC controllers.

Node	CMPC		AVC	
	Test1	Test2	Test1	Test2
3	807	689	834	650
5	−875	−317	−984	−318
7	999	501	1037	464
RMSE (%)	1.5	1.2	5.6	3.7

The controller performance in nodes 3, 5, and 7 was shown in the previous results, where VBBCs act to stabilize the microgrid according to the proposed predictive controller. In addition, there are constant power loads connected to nodes 2 and 8, where there are also VBBC that regulate the power regardless of the microgrid operation conditions. Thus, the sudden power change that occurs at 0.25 s is detected by the converters connected at nodes 2 and 8 to continue supplying the load with constant power. The current waveforms supplied by the converters to the load at nodes 2 and 8 during the sudden power change are shown in Figure 15. The timebase in Figure 15a,b are 100 ms/div and 10 ms/div, respectively. These figures show load current results before and after the sudden change that occur in 0.25 s. It can be noticed how each converter detects this change and stabilizes the constant power load current.

5. Conclusions

This paper proposes a CMPC of low computational effort that can achieve voltage or power regulation for DCMG stabilization. The prediction model is a matrix expression as a function of DCMG admittance. The admittance matrix is reduced to those DCMG nodes in which power is supplied or absorbed. The matrix model reduction and the one-step prediction horizon decrease the computational effort. The VBBC converter is proposed in this paper as the DC–DC stage for the supply and DC loads interconnection. The proposed CMPC and DCMG, using the VBBC converter, have been validated in an experimental setup based on HIL and compared with the AVC. Waveforms and numerical results demonstrate that the CMPC presents an excellent dynamic response and stable behavior. The CMPC performance is higher in start-up and power reference change tests, achieving settling times lower than 4 ms. The proposed controller is a generalized procedure that can be extended to larger DCMG independent of the converters used for the DC–DC conversion. Futures works will consider distributed control of the proposed predictive control using proximal algorithms and study the communication effects on the microgrid stability and performance.

Author Contributions: Conceptualization, D.M.-Y. and A.G.; investigation, D.M.-Y. and S.R.; methodology, D.M.-Y. and A.G.; project administration, C.R.; resources, C.R.; software, D.M.-Y., S.R. and C.G.-C.; supervision, C.R. and A.G.; validation, S.R. and C.G.-C.; visualization, S.R. and C.R.; writing-original draft, D.M.-Y.; writing-review and editing, C.G.-C. and A.G. All authors have read and agreed to the published version of the manuscript.

Funding: This work was supported by the Chilean Government under Projects (ANID/FONDECYT /3220126), (ANID/FONDECYT /1191680), Millenium Institute on Green Ammonia as Energy Vector MIGA (ANID / Millennium Science Initiative Program / ICN2021_023), SERC Chile (ANID/FONDAP /15110019), and (ANID/ PFECHA/Doctorado-Nacional/2019-21191663).

Institutional Review Board Statement: Not applicable.

Informed Consent Statement: Not applicable.

Data Availability Statement: Not applicable.

Conflicts of Interest: The authors declare no conflict of interest.

Abbreviations

The following abbreviations are used in this manuscript:

AVC	Average Voltage Control.
CMPC	Centralized Model Predictive Control.
CPLs	Constant Power Loads.
DCMG	DC Microgrid.
DER	Distributed Energy Resources.
ESS	Energy Storage Systems.
HIL	Hardware-In-The-Loop.
MPC	Model Predictive Control.
PCC	Point of Common Coupling.
PI	Proportional–Integral.
VBBC	Versatile Buck–Boost Converter.

Nomenclature

α	weighting factor.
A	intermediate matrix result.
c_n	n -node capacitor.
C	capacitance matrix.
g_n	n -node admittance.
g_{nm}	admittance joining node n to node m .
G	nodal admittance matrix.
i_n	n -node current.
I	identity matrix.
J	cost function.
k	current time instant.
M	total number of nodes.
n	n -node.
N	prediction horizon.
P	controlled power vector.
\bar{P}	reference value of P .
p_n	power source.
Q	definite matrix.
R	intermediate matrix result.
S	definite matrix.
T_s	sampling time.
V	node voltages vector.
\bar{V}	reference value of V .
u	control signal.
v_n	n -node voltage.
v_m	m -node voltage.
y	future output.
C^{-1}	inverse matrix.
$\frac{d}{dt}$	differentiation with respect to time.
$diag(V)$	diagonal matrix of V .

References

1. Al-Ammar, E.A.; Habib, H.U.R.; Kotb, K.M.; Wang, S.; Ko, W.; Elmorshedy, M.F.; Waqar, A. Residential Community Load Management Based on Optimal Design of Standalone HRES With Model Predictive Control. *IEEE Access* **2020**, *8*, 12542–12572. [[CrossRef](#)]
2. Guerrero, J.M.; Chandorkar, M.; Lee, T.L.; Loh, P.C. Advanced Control Architectures for Intelligent Microgrids—Part I: Decentralized and Hierarchical Control. *IEEE Trans. Ind. Electron.* **2013**, *60*, 1254–1262. [[CrossRef](#)]
3. Dragičević, T.; Lu, X.; Vasquez, J.C.; Guerrero, J.M. DC Microgrids—Part I: A Review of Control Strategies and Stabilization Techniques. *IEEE Trans. Power Electron.* **2016**, *31*, 4876–4891. [[CrossRef](#)]
4. Dragičević, T.; Lu, X.; Vasquez, J.C.; Guerrero, J.M. DC Microgrids—Part II: A Review of Power Architectures, Applications, and Standardization Issues. *IEEE Trans. Power Electron.* **2016**, *31*, 3528–3549. [[CrossRef](#)]

5. Qiu, R.; Liao, Q.; Yan, J.; Yan, Y.; Guo, Z.; Liang, Y.; Zhang, H. The coupling impact of subsystem interconnection and demand response on the distributed energy systems: A case study of the composite community in China. *Energy* **2021**, *228*, 120588. [[CrossRef](#)]
6. Fichera, A.; Marrasso, E.; Sasso, M.; Volpe, R. Energy, Environmental and Economic Performance of an Urban Community Hybrid Distributed Energy System. *Energies* **2020**, *13*, 2545. [[CrossRef](#)]
7. Schrittwieser, L.; Leibl, M.; Kolar, J.W. 99 Rectifier. *IEEE Trans. Power Electron.* **2020**, *35*, 138–157. [[CrossRef](#)]
8. Kumar, D.; Zare, F.; Ghosh, A. DC Microgrid Technology: System Architectures, AC Grid Interfaces, Grounding Schemes, Power Quality, Communication Networks, Applications, and Standardizations Aspects. *IEEE Access* **2017**, *5*, 12230–12256. [[CrossRef](#)]
9. Khezri, R.; Mahmoudi, A. Review on the state-of-the-art multi-objective optimisation of hybrid standalone/grid-connected energy systems. *IET Gener. Transm. Distrib.* **2020**, *14*, 4285–4300. [[CrossRef](#)]
10. Dragičević, T.; Guerrero, J.M.; Vasquez, J.C.; Škrlec, D. Supervisory Control of an Adaptive-Droop Regulated DC Microgrid With Battery Management Capability. *IEEE Trans. Power Electron.* **2014**, *29*, 695–706. [[CrossRef](#)]
11. Han, Y.; Zhang, K.; Li, H.; Coelho, E.A.A.; Guerrero, J.M. MAS-Based Distributed Coordinated Control and Optimization in Microgrid and Microgrid Clusters: A Comprehensive Overview. *IEEE Trans. Power Electron.* **2018**, *33*, 6488–6508. [[CrossRef](#)]
12. Saravi, S.V.S.; Sakhaei, H.; Kalantar, M.; Anvari-Moghaddam, A. A novel power management strategy based on combination of 3D droop control and EKF in DC microgrids. *IET Renew. Power Gener.* **2021**, *15*, 2540–2555. [[CrossRef](#)]
13. Khayat, Y.; Shafiee, Q.; Heydari, R.; Naderi, M.; Dragičević, T.; Simpson-Porco, J.W.; Dörfler, F.; Fathi, M.; Blaabjerg, F.; Guerrero, J.M.; et al. On the Secondary Control Architectures of AC Microgrids: An Overview. *IEEE Trans. Power Electron.* **2020**, *35*, 6482–6500. [[CrossRef](#)]
14. Hu, J.; Shan, Y.; Guerrero, J.M.; Ioinovici, A.; Chan, K.W.; Rodriguez, J. Model predictive control of microgrids—An overview. *Renew. Sustain. Energy Rev.* **2021**, *136*, 110422. [[CrossRef](#)]
15. Khalilzadeh, M.; Vaez-Zadeh, S.; Rodriguez, J.; Heydari, R. Model-Free Predictive Control of Motor Drives and Power Converters: A Review. *IEEE Access* **2021**, *9*, 105733–105747. [[CrossRef](#)]
16. Bordons, C.; Garcia-Torres, F.; Ridao, M.A. *Model Predictive Control of Microgrids*; Springer: Berlin/Heidelberg, Germany, 2020; Volume 358.
17. Vazquez, S.; Rodriguez, J.; Rivera, M.; Franquelo, L.G.; Norambuena, M. Model Predictive Control for Power Converters and Drives: Advances and Trends. *IEEE Trans. Ind. Electron.* **2017**, *64*, 935–947. [[CrossRef](#)]
18. Ni, F.; Zheng, Z.; Xie, Q.; Xiao, X.; Zong, Y.; Huang, C. Enhancing resilience of DC microgrids with model predictive control based hybrid energy storage system. *Int. J. Electr. Power Energy Syst.* **2021**, *128*, 106738. [[CrossRef](#)]
19. Marepalli, L.K.; Gajula, K.; Herrera, L. Fast Distributed Model Predictive Control for DC Microgrids. In Proceedings of the 2020 IEEE 21st Workshop on Control and Modeling for Power Electronics (COMPEL), Aalborg, Denmark, 9–12 November 2020; pp. 1–6. [[CrossRef](#)]
20. Abbasi, M.; Dehkordi, N.M.; Sadati, N. Decentralized Model Predictive Voltage Control of Islanded DC Microgrids. In Proceedings of the 2020 11th Power Electronics, Drive Systems, and Technologies Conference (PEDSTC), Tehran, Iran, 4–6 February 2020; pp. 1–6. [[CrossRef](#)]
21. Karami, Z.; Shafiee, Q.; Sahoo, S.; Yaribeygi, M.; Bevrani, H.; Dragicevic, T. Hybrid Model Predictive Control of DC–DC Boost Converters With Constant Power Load. *IEEE Trans. Energy Convers.* **2021**, *36*, 1347–1356. [[CrossRef](#)]
22. Navas-Fonseca, A.; Burgos-Mellado, C.; Espina, E.; Rute, E.; Gómez, J.S.; Sáez, D.; Sumner, M. Distributed Predictive Secondary Control for Voltage Restoration and Economic Dispatch of Generation for DC Microgrids. In Proceedings of the 2021 IEEE Fourth International Conference on DC Microgrids (ICDCM), Arlington, VA, USA, 18–21 July 2021; pp. 1–6. [[CrossRef](#)]
23. Hidalgo-Rodríguez, D.I.; Myrzik, J. Optimal Operation of Interconnected Home-Microgrids with Flexible Thermal Loads: A Comparison of Decentralized, Centralized, and Hierarchical-Distributed Model Predictive Control. In Proceedings of the 2018 Power Systems Computation Conference (PSCC), Dublin, Ireland, 11–15 June 2018; pp. 1–7. [[CrossRef](#)]
24. Hajar, K.; Hably, A.; Bacha, S.; Elrafhi, A.; Obeid, Z. An application of a centralized model predictive control on microgrids. In Proceedings of the 2016 IEEE Electrical Power and Energy Conference (EPEC), Ottawa, ON, Canada, 12–14 October 2016; pp. 1–6. [[CrossRef](#)]
25. Wang, R.; Xiao, G.; Wang, P. Hybrid Centralized-Decentralized (HCD) Charging Control of Electric Vehicles. *IEEE Trans. Veh. Technol.* **2017**, *66*, 6728–6741. [[CrossRef](#)]
26. Babqi, A.J.; Yi, Z.; Etemadi, A.H. Centralized finite control set model predictive control for multiple distributed generator small-scale microgrids. In Proceedings of the 2017 North American Power Symposium (NAPS), Morgantown, WV, USA, 17–19 September 2017; pp. 1–5. [[CrossRef](#)]
27. Serban, I.; Céspedes, S.; Marinescu, C.; Azurdia-Meza, C.A.; Gómez, J.S.; Hueichapan, D.S. Communication Requirements in Microgrids: A Practical Survey. *IEEE Access* **2020**, *8*, 47694–47712. [[CrossRef](#)]
28. Song, J.; Jung, S.; Lee, J.; Shin, J.; Jang, G. Dynamic performance testing and implementation for static var compensator controller via hardware-in-the-loop simulation under large-scale power system with real-time simulators. *Simul. Model. Pract. Theory* **2021**, *106*, 102191. [[CrossRef](#)]
29. Ramírez-Murillo, H.; Restrepo, C.; Calvente, J.; Romero, A.; Giral, R. Energy Management DC System Based on Current-Controlled Buck-Boost Modules. *IEEE Trans. Smart Grid* **2014**, *5*, 2644–2653. [[CrossRef](#)]

30. Ramírez-Murillo, H.; Restrepo, C.; Calvente, J.; Romero, A.; Giral, R. Energy Management of a Fuel-Cell Serial–Parallel Hybrid System. *IEEE Trans. Ind. Electron.* **2015**, *62*, 5227–5235. [[CrossRef](#)]
31. González-Castaño, C.; Restrepo, C.; Kouro, S.; Vidal-Idiarte, E.; Calvente, J. A Bidirectional Versatile Buck–Boost Converter Driver for Electric Vehicle Applications. *Sensors* **2021**, *21*, 5712. [[CrossRef](#)] [[PubMed](#)]
32. Restrepo, C.; Gonzalez-Castano, C.; Giral, R. The Versatile Buck-Boost Converter as Power Electronics Building Block: Changes, Techniques, and Applications. *IEEE Ind. Electron. Mag.* **2022**. [[CrossRef](#)]
33. Dorfler, F.; Bullo, F. Kron Reduction of Graphs With Applications to Electrical Networks. *IEEE Trans. Circuits Syst. I Regul. Pap.* **2013**, *60*, 150–163. [[CrossRef](#)]
34. Murillo-Yarce, D.; Garcés-Ruiz, A.; Escobar-Mejía, A. Passivity-Based control for DC-Microgrids with constant power terminals in island mode operation. *Rev. Fac. Ing. Univ. Antioq.* **2018**, *86*, 32–39. [[CrossRef](#)]
35. Xu, Q.; Vafamand, N.; Chen, L.; Dragičević, T.; Xie, L.; Blaabjerg, F. Review on Advanced Control Technologies for Bidirectional DC/DC Converters in DC Microgrids. *IEEE J. Emerg. Sel. Top. Power Electron.* **2021**, *9*, 1205–1221. [[CrossRef](#)]
36. Restrepo, C.; Calvente, J.; Cid-Pastor, A.; Aroudi, A.E.; Giral, R. A Noninverting Buck–Boost DC–DC Switching Converter With High Efficiency and Wide Bandwidth. *IEEE Trans. Power Electron.* **2011**, *26*, 2490–2503. [[CrossRef](#)]
37. Restrepo, C.; Konjedic, T.; Flores-Bahamonde, F.; Vidal-Idiarte, E.; Calvente, J.; Giral, R. Multisampled Digital Average Current Controls of the Versatile Buck–Boost Converter. *IEEE J. Emerg. Sel. Top. Power Electron.* **2018**, *7*, 879–890. [[CrossRef](#)]
38. Zamiri, E.; Sanchez, A.; Yushkova, M.; Martínez-García, M.S.; de Castro, A. Comparison of Different Design Alternatives for Hardware-in-the-Loop of Power Converters. *Electronics* **2021**, *10*, 926. [[CrossRef](#)]